DOI 10.24412/2221-2574-2022-2-20-29 УДК 621.396

ОЦЕНКА 10-ПАНЕЛЬНОГО ДЕМОНСТРАТОРА С ПОМОЩЬЮ ПОГОДНЫХ ДАННЫХ

Душан Зрнич
PhD, академик, старший научный сотрудник, адьюнкт-профессор, Национальная лаборатория по исследованию сильных штормов[1], Университет Оклахомы[2], США.
E-mail: Dusan.Zrnic@noaa.gov

Леся Боровска
PhD, постдок, Университет Оклахомы[2], США.
E-mail: Lesya.Borowska@noaa.gov

[1]*Адрес:* 120 David L Boren Blvd., Norman, Oklahoma, USA, 73072
[2]*Адрес:* 660 Parrington Oval, Norman, Oklahoma, USA, 73019.

Аннотация: В данной статье содержится оценка 10-панельного демонстратора (TPD) — поляризационного радара с фазированной антенной решёткой. Основная цель статьи – проинформировать пользователей атмосферных радаров о проблемах использования технологии фазированных антенных решёток (ФАР) при наблюдениях за погодой. В статье описывается пример наблюдения шторма с помощью TPD-радара. Измерялись спектральные моменты и дифференциальная фаза, которые сравнивались с соответствующими параметрами, измеренными с помощью прототипа радара WSR-88D, также известного под именем NEXRAD. На данной стадии разработки ФАР главными проблемами являются ошибки в измерении поляризационных параметров и стабильность системы. Они и оцениваются путем сравнения.

Ключевые слова: поляризационный радар, фазированная антенная решетка, метеорологические наблюдения, фазированная антенная решётка, стабильность системы.

1. Introduction

The US national network of weather radars consists of some 155 polarimetric Doppler weather radars. Because these have reached the end of designed life time, the National Weather Service (NWS) begun overhauling the critical components hoping to extend the lifetime by 15 to 20 years. Although this seems distant, researchers have started to look at replacements with a newer and better technologies. A promising replacement is the PAR and the National Severe Storms Laboratory (NSSL) initiated investigation of this technology in 2004 on a PAR that had Doppler capability but no dual polarization [1]. The radar demonstrated detections of rapidly evolving phenomena like tornadoes and downbursts.

The next steps in the PAR research were studies of polarimetric capabilities and it became clear that achieving the polarimetric performance of the WSR-88D would be hard to match. To achieve this goal, the NSSL and the Federal Aviation Administration engaged the MIT Lincoln Laboratory to build the TPD. Its copolar and cross-polar antenna patterns at broadside are presented in [2].

2. The Ten Panel Demonstrator

The TPD (fig. 1) is a phased-array radar with dual polarization capability. It consists of ten panels each with 64 radiating elements grouped in 8 overlapping subarrays. For easy deployment it is mounted on a trailer and can be positioned to point at any direction with respect to the trailer. Before operations, the trailer needs to be leveled and the atnenna pointed in a desired direction. Moreover, for verical orientation either the longer or shorter side of the aperature can be aligned parallel to the ground. Various characteristics of the TPD radar are listed in Table 1, together whith those of the research WSR-88D radar (designated as KOUN). The TPD uses pulse compression to increase detectability. The super resolution on the KOUN refers to sampling in azimuth at half the beamwidh. The TPD beamwidth in azimuth and elevation refer to the antenna oriented so that its shorter dimenstion is parallel to the ground. In the experiment the TPD broadside beam was centered at 236° and scanned the sector of 80°. Three consecutive radials of TPD are collected within its beamwidth whereas twelve radials of the KOUN

(a) (b)

Fig. 1. The Ten Demonstrator Radar: (a) view from the front, the antenna longer side is parallel parallel to the ground and (b) view from the back. The element are grouped in 8 overlapping subarray.

are collected. As seen in the table, the TPD collected two scans in elevation while the KOUN collected 5 scans.

Because the TPDs peak-transmitted power is weak, the radar's detectability is low; a 20 dBZ reflectivity (Z) produces an SNR of 0 dB at 25 km. For the KOUN the Z of –16 dBZ at the same distance equals the noise power. That is, KOUN has a 36 dB better detectability. Therefore, in scan strategies of TPD, we used pulse compression.

Table 1: Radar parameters of TPD and KOUN

Parameter	TPD	KOUN
Mode	Pulse compression	Super resolution
Frequency	2.87 GHz	2.705 GHz
Peak transmitted power	3 kW	750 kW
Pulse length, τ	20 μs	1.57 μs
Compression ratio	10	N/A
Compressed pulse	2 μs	N/A
Linear FM Δf	330 kHz	N/A
Weighting	Hamming	N/A
PRT	1 ms	1 ms
Number of pulses	128	64
Beamwidth	Az =6.3° ; El = 2.5°	0.95°
Center azimuth angle	236°	N/A
Azimuth sector	80°	172°
Steps in azimuth	2°	0.5°
Elevation scans	1°, 2°	0.9°, 1.4°, 1.8°, 2.2°, 2.7°
Range step	48 m	250 m

The waveform we chose is a linear Frequency Modulation (FM expressed as

$$s(t) = A(t)\exp\left\{2\pi j\left[\left(f_0 - \Delta f/2\right)t + \Delta f t^2/2T\right]\right\}, \quad (1)$$

where A(t) is the tapered amlitude (herein the Hamming window), T is the pulse duration and Δf is the frequency deviation; the equation is valid for $t \le T$. We chose the frequency deviation Δf = 0.33 MHz (table 1) because it produces the same range resolution (300 m, fig. 2) as the scan without pulse compression and pulse length τ = 2 μs which is convenient for comparisons with KOUN data.

For comparisons with the KOUN radar, we had deployed the TPD 100 m from the KOUN. The TPD records time series (I, Q) data from 8 subarrays. Therefore, at horizontal polarization there are 8 channels of (I, Q) time series data and 8 channels at vertical polarization. The distributed oscillators in the TPD were not sufficiently stable; therefore, we compensated the time series data for the instabilities as follows. At the end of each dwell time we injected the local oscillator's signal into the receiver and recorded the phases of the (I, Q) signals which were then taken out of the weather signals. Thereafter, we processed the data and calculated the spectral moments (reflectivity, Doppler velocity, and spectrum width) and the polarimetric

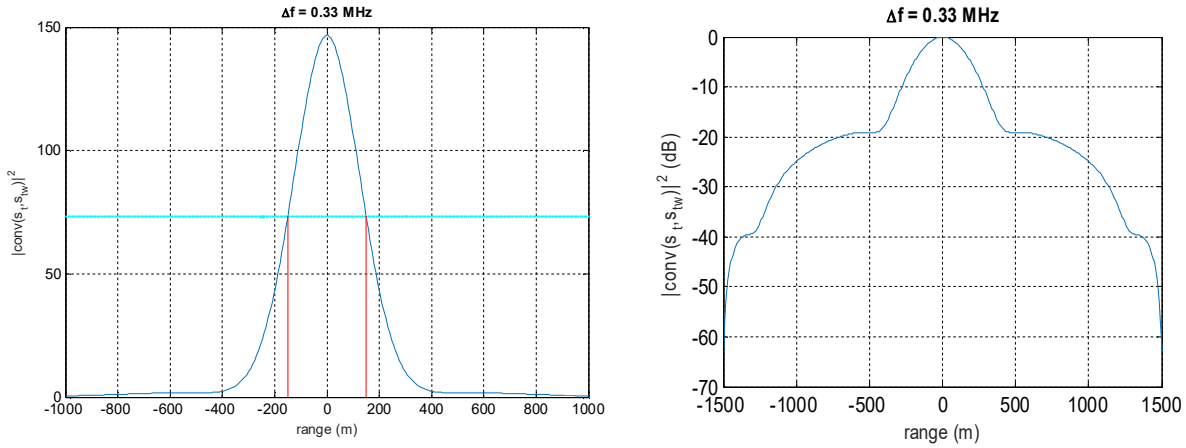

(a) (b)

Fig. 2. (a) Range weighting function of the compressed pulse with applied Hamming window. The plot extends up to 1000 m. The frequency band, Δf, is 0.33 MHz. (b) Same as in Fig. 2a, but in log units normalized by the peak power. Values in range up to 1500 m are plotted out of the total 3000 m.

variables (differential reflectivity, correlation coefficient, and differential phase) according to the formulas in Doviak and Zrnic [3]. The data from the KOUN are the so called level II (spectral moments and polarimetric variables). An SNR coherency threshold [4], ground clutter filter, interference and point clutter filters have been applied on the data prior to recording the variables.

One more consideration is the pair of elevation angles from which data of the two radars should be compared. This is because the beamwidths in elevation differ and so do the beam blockages. From the heights of the two antennas, a survey of KOUN, and the surface objects depiction on the Google Earth we determined the following. Between the azimuths of 200° and 270° the elevation angle on the KOUN is blocked up to 0.1°. The beam blockage of the TPD antenna extends to 1°. By examining the velocity fields of the two radars we established that at the elevation of 1.8° for KOUN and 1° for TPD the fields matched best. The physical explanation is in fig. 3 where the beam cross sections at indicated elevation angles are plotted. The beam shapes are Gaussian with appropriate width determined by the beamwidths [3].

It is clear from fig. 3 that only the top half of the KOUN beam at 1° elevation overlaps with the TPD weighting function at its lowest elevation (1°). The bottom half of KOUN beam samples scatterers to which the TPD is blind. The KOUN beam at 1.8° elevation almost fully overlaps the TPD beam. We have available a KOUN beam at 1.4° and its velocity fields do not agree with the TPD field as the one from the 1.8° elevation scan. Therefore, we compare the fields at scans from these two elevation angles.

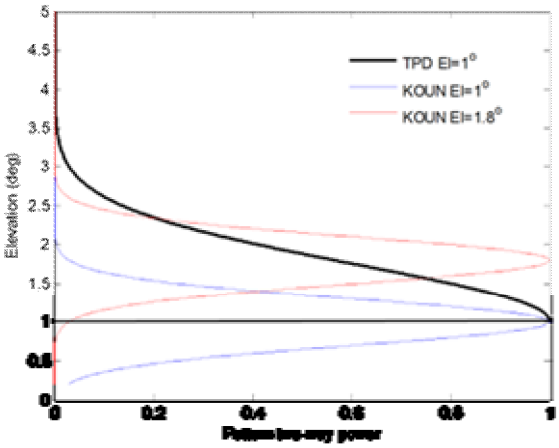

Fig. 3. Two-way power patterns. The black curve is for TPD elevation angle of 1o. The horizontal line at 1o indicates the blockage, hence to a good approximation the black graph is the elevation weighting function of the TPD. The color curves are the weighting functions of the KOUN at indicated elevation angles. The KOUN's antenna is on a 25 m tower hence its beams at elevations larger than 1o are not blocked.

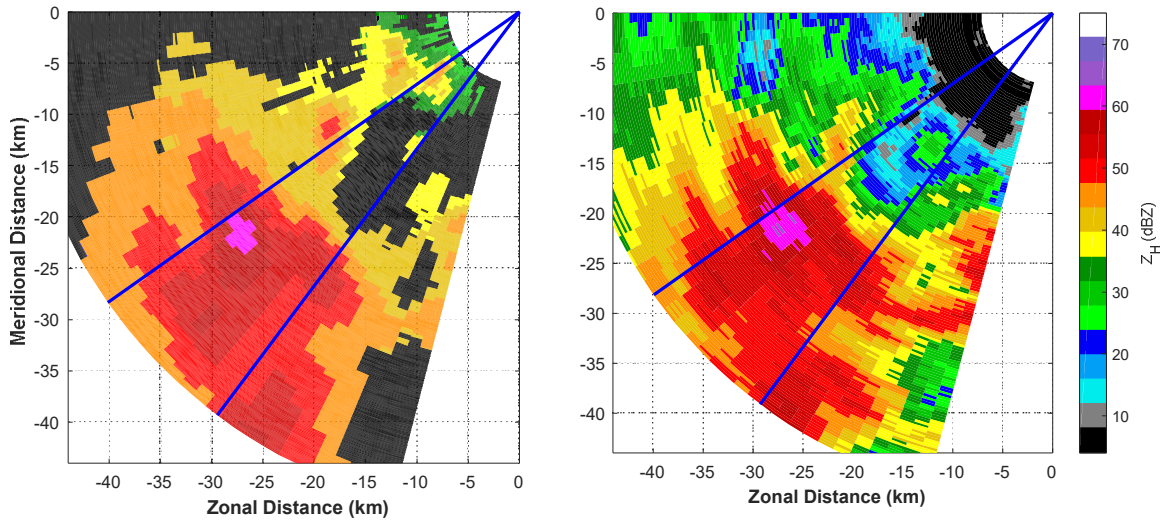

Fig. 4. a) Reflectivity field over a sector scanned with the TPD at elevation equal 1°. b) Same as (a), but with KOUN at elevation equal 1.8°. The color bar on the right indicates Z values in dBZ. Scans made at 1759 UTC, on 15 May 2018. An SNR threshold of 2 dB is applied to the TPD data.

3. Weather Observations

On 15th of May 2018, we collected several data sets with the TPD and the KOUN radars. The data have been recorded almost simultaneously (within 59 s) and scanning radar parameters are in table 1. The range and azimuth steps as well as the beam widths differ on these radars. Therefore, on KOUN data we applied an 11-point mean filter (5.5°) in the azimuth direction and plotted data at 2° increments. We used 42-point median filter (2015 meters) in range for each TPD's radial of data.

Our comparisons revealed that the differential reflectivity Z_{DR} and the copolar to cross-polar correlation coefficient ρ_{hv} can't be measured reliably due to system instabilities. Hence in the sequel we present measurements of the reflectivity Z, differential phase Φ_{DP}, Doppler velocity v, and Doppler spectrum width σ_v.

3.1 *Reflectivity*

In principle, the reflectivity can be computed from the weather radar equation and in the appendix we present a heuristic derivation of the equation for the PAR. However, in case of the TPD it is very difficult to determine the transfer function of the antenna backend and precise shapes of the patterns on transmission and reception. Therefore, we compared the reflectivity fields of the TPD with those of the KOUN as follows. We identified area where the TPD and KOUN beams overlapped and obtained the radar constant. It turns out that the constants C at 1° and 2° scans are 22.6 and 18.6 dB. The reflectivity is then

$$Z_h = P_h + 20\log(r) - C - \\ - 10\log[\cos(az_b - az)], \qquad (2)$$

where the P_h is the recorded power, r is range (km), az_b is the azimuth at broadside, and az is the azimuth at which the beam is pointing. The cosine dependence accounts for the beamwidth and gain change off broadside (appendix). However, we did not include the gain change due to the element pattern, which in our case is insignificant because that gain is almost constant over ±25° [5]. We ignore the similar dependence in elevation because at 2° it is less than 0.003 dB.

Figs. 4a and 4b depict the fields of Z_h measured by the TPD and KOUN from conical PPI scans at 1° elevation (TPD) and 1.8° elevation (KOUN) at 1759 UTC on 15 May 2018. The precipitation band is characterized by high Z_h (exceeding 55 dBZ) and Z_{DR} over 3–4 dB. Comparing figs. 4a and 4b between the two blue solid lines, we notice similar shape of the area with the high values of Z_h. The TPD's reflectivity factor Z_h is about 2 dB

lower and overwhelmed by noise at Z_h lower than 35 dBZ and distance from the radar larger than 10 km compared to the KOUN's reflectivity. This is explained by the large beamwidth (incomplete beam filling results in lower Z values) and low TPD detectability.

Next we examine the histograms of the reflectivities from the two radars (fig. 5). Comparison reveals general agreement and some significant differences. The lack of TPD data below 40 dBZ is a consequence of low detectability (sensitivity). We have no definite explanation of the bimodal nature of the Z histogram from TPD or the suspicious dip in values between 42 and 45 dBZ. Nonetheless, because the TPD beam is very wide the contribution by ground clutter is significant and might have caused the second peak.

The significant Φ_{DP} from the TDP span a wider azimuthal sector likely because its beamwidth is about 12 times larger the one of the KOUN. Therefore, it samples precipitation from wider span of altitudes than the KOUN. Depending on vertical profile of reflectivity, the beam-weighted values can be larger or smaller. What matters are the Φ_{DP} radial gradients because these are used to compute rain rate estimates [6]. The gradients are comparable suggesting that rain rate estimates would be acceptable.

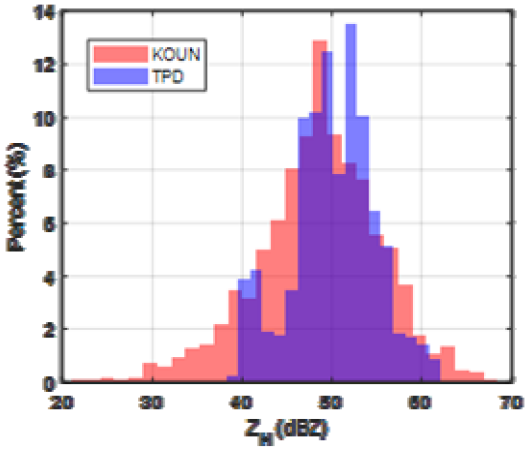

Fig. 5. Histograms of the reflectivity at horizontal polarization. The data are from within the angular sectors in fig. 3 and from 24 km to the end.

3.2 *Doppler velocities*

In figures, 7a and 7b are the Doppler velocity fields measured with TPD and KOUN. The fields are very similar in patterns and values at area where the SNR values on the TPD are significant. Evidently, the TPD estimates fairly well the mean Doppler velocities. This is rooted in the robustness of the phase measurement. Some differences we attribute to the tremendous difference in beam cross sections. Although we

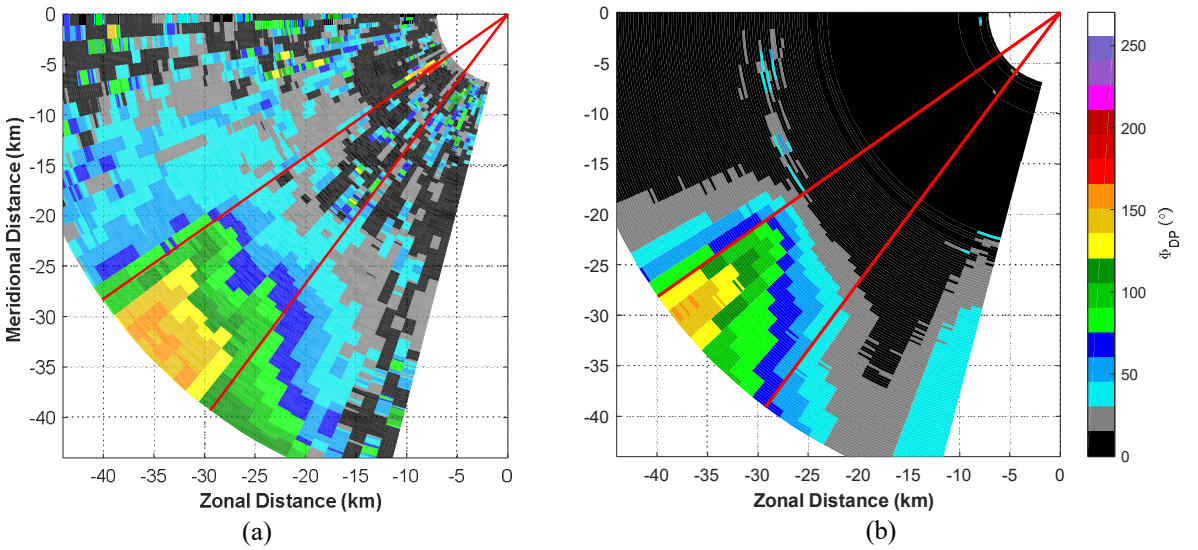

Fig. 6. (a) Differential phase, Φ_{DP} field over a sector scanned with the TPD radar at elevation 1°. (b) Same as (a), but over a sector scanned with KOUN at elevation 1.8°. The color bar on the right indicates values of Φ_{DP} in degrees.

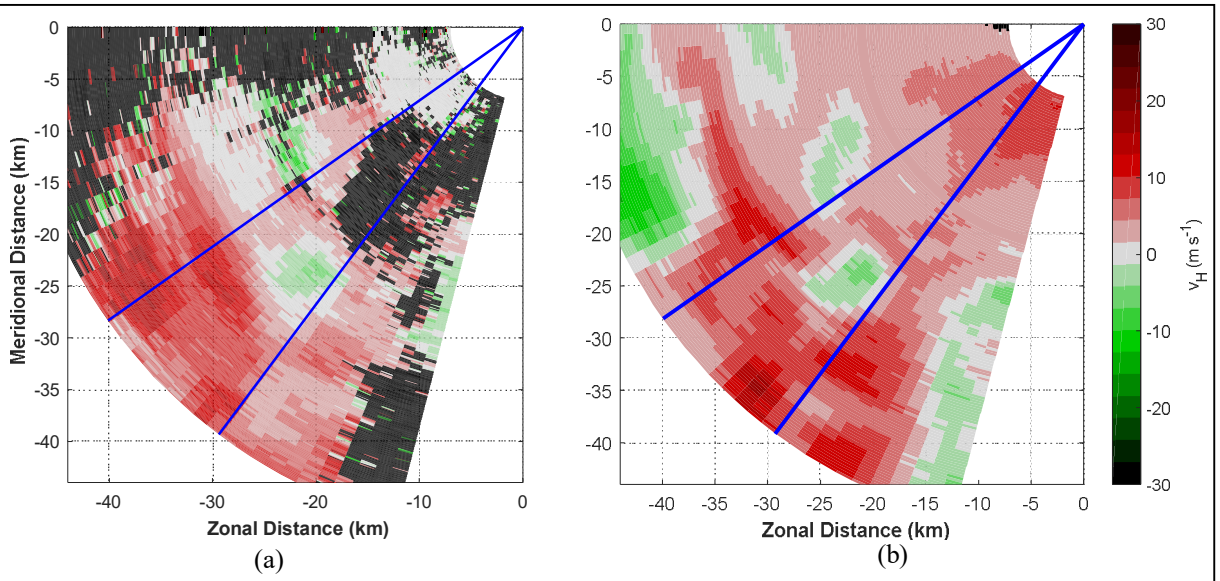

Fig. 7. (a) Velocity field over a sector scanned with the TPD radar at elevation 1°. (b) Same as (a), but over a sector scanned with the KOUN radar at elevation 1.8°. The black areas in the TPD field are below the SNR threshold. The color bar on the right indicates contours of Dopler velocities in m s^{-1}.

have averaged data in azimuth, the effective beam shape of the TPD (including blockages) is significantly different. Moreover, in elevation, there is no easy way to match the beams because the scans are offset in time.

The histograms (fig. 8) point out the differences which are not evident in the fields (fig. 7). Note the bimodal shape of the velocity histogram from the TPD. A hint of similar feature is present in the histogram of reflectivity *Z* (fig. 5).

3.3 *Doppler spectrum widths*

Figure 9 exhibits the Doppler spectrum width fields from the TPD's (fig. 9a) and KOUN's (fig. 9b) measurements. The fields differ in values and the ones from the TPD are larger. A possible reason could be the broader beamwidth of the TPD. Therefore, the TPD catches more variations of the wind caused by shear and turbulence. To demonstrate the similarity in patterns we have reduced the spectrum widths in fig. 9a by multiplying these with 0.55 (fig. 9c). Clearly, the pattern of the reduced spectrum widths is similar to the pattern from the KOUN observation (fig. 9b).

4. Conclusion

The weather data collected with the polarimetric TPD radar are the first of its kind because it is the first built 10-cm wavelength, phased array radar with dual polarization capability. Our examination of the fields of reflectivity, differential phase, Doppler velocity, and spectrum width revealed the issues and virtues of the TPD. As the TPD serves to prove some concepts and educate the designers and developers of potential problems, we are pleased to state that the TPD

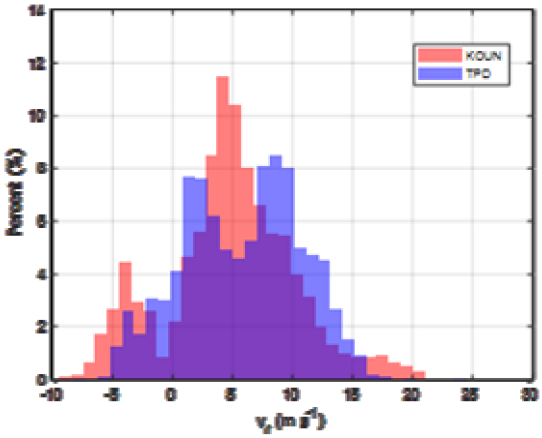

Fig. 8. Histograms of the Doppler velocities. The data are from within the angular sectors in fig. 7 and between 24 km and the end of scan.

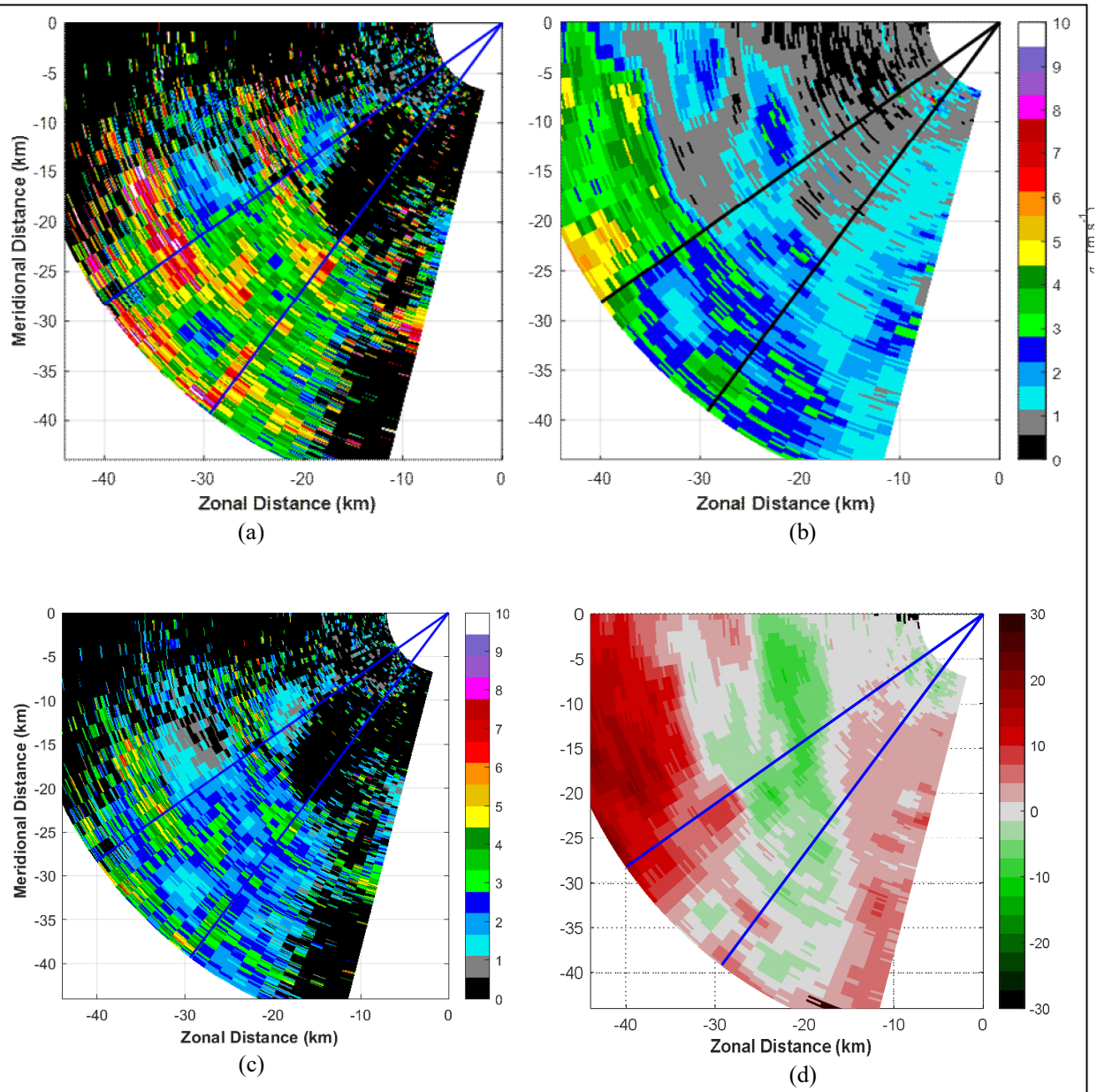

Fig. 9. (a) Doppler spectrum width field scanned with the TPD radar at elevation 1°. (b) Same as (a), but scanned with the KOUN radar at elevation 1.8°. c) Same as in (a) but the spectrum widths are multiplied by 0.55. d) Velocity difference field. It is the difference of the velocities at 0.9° and 1.8°, both measured with the KOUN radar. The difference is proportional to the vertical shear of the Doppler winds.

functions as a weather observing radar. Its fields of velocities agree well with the ones from KOUN. So do the fields of reflectivity. The fields of spectrum width have a high bias, but the features (patterns) are preserved suggesting that removing bias may be possible. Therefore, the radar has potential for quantitative observation of weather similar to non-polarimetric weather radars.

The radar also can make good measurements of differential phase. Of all the variables, the Doppler velocity and differential phase are the most robust. This is expected as these measurements use the phases of the weather signals. Noises, nonlinearities, and other artifacts affect much less the signal's phases than amplitudes.

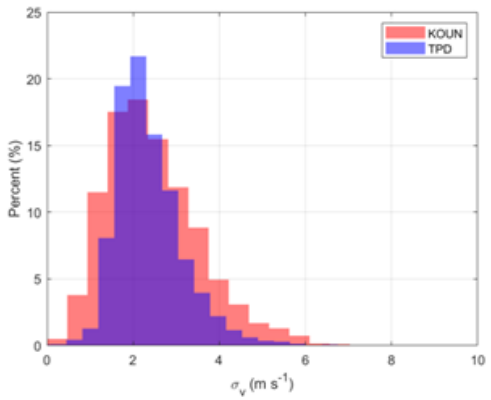

Fig. 10 Histograms of the Doppler spectrum widths. The data are from within the angular sectors in fig. 9b and c, and from 24 km to the end of scan.

The field of differential phase looks reasonable. Comparison of values with the nearby WSR-88D indicates general agreement. Some difference in span is explained by the effects of beam smoothing inherent to the wider beamwidth of the TPD radar. The TPD's radial profile of differential phase agrees in slope and values with the KOUN's one. This means that rain measurements based on the differential phase would be good. Moreover, adequate measurements of rain from estimates of the attenuation is possible as well as correction of attenuated powers.

The SNRs in these data are less than about 15 dB, which is unfavorable to the accuracy of the measurements. The current TPD has instabilities originating possibly in the active components. Hence, we could not reliably estimate the differential reflectivity or correlation coefficient. This by itself is not a deficiency because the TPD's purpose is neither scientific nor operational application. It is a platform on which to test multiple facets of weather observation by polarimetric PARs. The TPD has served this role and influenced the development of the Advanced Technology Demonstrator [4].

Acknowledgments

D. Wasielewski, A. Zahrai, M. Shattuck, and M. Schmidt maintained the TPD and helped with data collection. I. Ivic gave advice on data processing and provided fig.8. L. Borowska was supported by NOAA/Office of Oceanic and Atmospheric Research under NOAA-University of Oklahoma Cooperative Agreement # NA21OAR4320204, U.S. Department of Commerce.

Appendix

Radar equation for the PAR

The radar equation for the PAR at the broadside is very similar to Doviak and Zrnic ([3], eq. 4.34) except the different gains on transmission and reception must be accounted for. In the case of a rectangular vertically oriented array, the beamwidth in the H and E planes differ. Start with the equation for broadside

$$P_r(r_o) = \frac{\pi^3 P_t\, g_t g_r \theta_a \theta_b c\tau |K_w|^2 Z_e}{2^{10}(\ln 2)\lambda^2 r^2 l_r}, \qquad (6)$$

where g_t, g_r are the effective gains of the transmitted beam and receiving beam, and θ_a, θ_b are the 3 dB beamwidths at broadside corresponding to the long a and short b dimensions of the panel.

Transmitted power is P_t, τ is the pulse length, $|K_w|^2$ is a factor that depends on the refractive index of water and at microwave frequencies, it is between 0.91 and 0.93, and l_r is the cumulative loss (larger than unity). The beamwidths are of the composite two-way pattern computed as a product of the voltage pattern on transmission with the voltage pattern on reception. With no loss of substance, we ignore propagation losses through the atmosphere and the gain transfer g_s relating the power at the antenna to the voltages in the receiver.

Next, we adjust (6) to accommodate beam pointing in directions other than the broadside. First consider isotropic radiators (elements) so that the only dependence in returned power is due to the reduction of the antenna effective area and concomitant increase in beamwidth. The reduced effective area A_{reff} equals the projection of the effective area at broadside A_{eff} on the polarization plane i.e.,

$$A_{\text{reff}} = A_{\text{eff}} \cos(az) \cos(el), \qquad (7)$$

where az and el are azimuths and elevations relative to the broadside beam axis of a vertically ori-

ented array antenna. The gains are also reduced and the beamwidth product is inversely proportional to the A_{reff}. This means that for pointing at *az, el* the product $\theta_a\theta_b$ in (6) should be replaced with $\theta_a\theta_b / [\cos(az)\cos(el)]$ and the product g_t g_r with $g_t\, g_r[\cos(az)\cos(el)]^2$.

We need one more step to complete the derivation. Recall that we assumed isotropic radiators. To account for the element pattern's gain variation with pointing direction we take the ratio squared of the gain $g_e(az, el)$ to the gain at broadside g_e and incorporate it into (6). The final result is the following radar equation

$$P_r(r_o) = \frac{\pi^3 P_t\, g_t g_r g_e^2(az,el)}{2^{10}(\ln 2) g_e^2 \lambda^2 r^2 l_r} \times$$

$$\times \cos(az)\cos(el)\theta_a\theta_b c\tau \left|K_w\right|^2 Z_e. \qquad (8)$$

This equation is identical to the one derived by Knorr [7] who started with fundamental principles and derived radar equations for frequency agile and phased array weather radars. In practice rather than separating the element pattern gains it may be easier to measure the gains and beamwidth at various pointing directions. In that case the measured values would replace the ones in (8) and the angular dependence would be implicit in the measured parameters.

Литература

1. *Zrnic, D.S., Kimpel J.F., Forsyth D.F., Shapiro A., Crain G., Ferek R., Heimmer J., Benner W., McNellis T.J., Vogt R.J.* Agile beam phased array radar for weather observations. Bull. Amer. Meteorol. Soc. 2007. Vol. 88. Pp. 1753–1766.
2. *Миркович Д., Зрнич Д.С.* Поляризационные радары с фазированной антенной решёткой для метеорологических наблюдений: состояние и проблемы // Радиотехнические и телекоммуникационные системы. 2019. № 2. С. 5–14.
3. *Doviak R.J., Zrnic D.S.* Doppler radar and weather observations. Mineola, New York: Dover Pub. Inc., 2006. 562 p.
4. *Ivić I., Schvartzman D.* A first look at the ATD data corrections. 39th Int. Conf. on Radar Meteorology. AMS, Nara, Japan. 2019.
5. *Mirkovic, Dj., Zrnic D.S.* Computational Electromagnetic Tools Applied to the Polarimetric Phased Array Antenna. NSSL report. 2019. [Electronic source] URL: https://nssl.noaa.gov/publications/mpar_reports/
6. *Ryzhkov A.V., Zrnic D.S.* Radar Polarimetry for Weather Observations. Cham, Switzerland: Springer, 2019. 486 p.
7. *Knorr J. BV.* Weather radar equation correction for frequency agile and phased array radars. IEEE Tr. on Aerospace and Electronic Syst. 2007. Vol. 43. Pp. 1220–1227.

Поступила 8 февраля 2022 г.

English

EVALUATION OF THE TEN PANEL DEMONSTRATOR (TPD) ON WEATHER DATA

Dusan S. Zrnic — PhD, Adjunct Professor, the National Severe Storms Laboratory[1], University of Oklahoma[2].
E-mail: Dusan.Zrnic@noaa.gov

Lesya Borowska — PhD, Postdoctoral Fellow, University of Oklahoma[2].
E-mail: Lesya.Borowska@noaa.gov

[1]*Address*: 120 David L Boren Blvd., Norman, Oklahoma, USA, 73072.
[2]*Адрес:* 660 Parrington Oval, Norman, Oklahoma, USA, 73019.

Abstract: This paper presents an evaluation of the Ten Panel Demonstrator (TPD), a Phased Array Radar (PAR) with dual-polarization capability. Its main purpose is to inform the atmospheric science and weather radar users about critical issues and challenges the PAR technology presents for observing weather. The paper contains sample measurements of a storm obtained with the TPD radar. Measured are the spectral moments and the differential phase; these are compared to those obtained with the research version of the Weather Surveillance Radar 1988 Doppler (WSR-88D) also known as NEXRAD. At this stage of PAR development, the principal issues are biases in the polarimetric variables and the stability of the radar system. These are addressed through the comparisons.

Keywords: polarizing radar, phased array antenna, meteorological observations.

References

1. *Zrnic, D.S., Kimpel J.F., Forsyth D.F., Shapiro A., Crain G., Ferek R., Heimmer J., Benner W., McNellis T.J., Vogt R.J.* Agile beam phased array radar for weather observations. Bull. Amer. Meteorol. Soc. 2007. Vol. 88. Pp. 1753–1766.

2. *Mirkovic Dj.*, *Zrnic D.S.* Polarimetric phased-array radar for weather observations: status and challenges. Radio and Telecommunication Systems. 2019. No. 2. Pp. 5–14.

3. *Doviak R.J., Zrnic D.S.* Doppler radar and weather observations. Mineola, New York: Dover Pub. Inc., 2006. 562 p.

4. *Ivić I., Schvartzman D.* A first look at the ATD data corrections. 39th Int. Conf. on Radar Meteorology. AMS, Nara, Japan. 2019.

5. *Mirkovic, Dj., Zrnic D.S.* Computational Electromagnetic Tools Applied to the Polarimetric Phased Array Antenna. NSSL report. 2019. [Electronic source] URL: https://nssl.noaa.gov/publications/mpar_reports/

6. *Ryzhkov A.V., Zrnic D.S.* Radar Polarimetry for Weather Observations. Cham, Switzerland: Springer, 2019. 486 p.

7. *Knorr J.BV.* Weather radar equation correction for frequency agile and phased array radars. IEEE Tr. on Aerospace and Electronic Syst. 2007. Vol. 43. Pp. 1220–1227.